arXiv:1007.4812v2 [hep-ph] 21 Dec 2010

LPT-10-52

Exploring SUSY light Higgs boson scenarios via dark matter experiments.

Debottam Das[1], Andreas Goudelis[1], Yann Mambrini[1]

[1]*Laboratoire de Physique Théorique d'Orsay, UMR8627–CNRS,*
Université Paris–Sud, Bât. 210, F–91405 Orsay Cedex, France

E-mails: `debottam.das@th.u-psud.fr`, `andreas.goudelis@th.u-psud.fr`,
`yann.mambrini@th.u-psud.fr`

Abstract

We examine the dark matter phenomenology in supersymmetric light higgs boson scenarios, adapting nonuniversal Higgs masses at the gauge coupling unification scale. The correct relic density is obtained mostly through the annihilation into a pseudoscalar A, which gives high values for the self-annihilation cross-section at present times. Our analysis shows that most part of the A pole region can produce detectable gamma-rays and antiproton signals, and still be compatible with with recent direct detection data from XENON100 and CDMS-II.

Contents

1 Introduction **2**

2 The NUHM and low energy constraints **4**

3 Direct Detection of Dark Matter **6**

4 Indirect Detection of Dark Matter **7**

- 4.1 Gamma-ray Detection 8
  - 4.1.1 The flux at intermediate latitudes 8
  - 4.1.2 The Fermi 1-year observations 9
- 4.2 Antiproton Detection 10
  - 4.2.1 Differential Event Rate 10
  - 4.2.2 The background and antiproton detection with AMS-02 12

5 Results and Discussion **13**

- 5.1 Cold Dark Matter Constraint and Light Higgs Boson Scenario 13
- 5.2 Exclusion and Detectability 15
- 5.3 Indirect Detection results 16

6 Discussion on the constraints from Direct Detection experiments **20**

7 Conclusions **23**

1 Introduction

Low energy supersymmetry (SUSY) [1], has emerged as the most promising candidate for physics beyond the Standard Model (SM). The minimal supersymmetric standard model (MSSM) has been attractive for its explanations towards several phenomena such as (i) the Higgs mass hierarchy problem in the SM, (ii) electroweak (EW) symmetry breaking via radiative corrections and (iii) the unification of the SM gauge couplings at the grand unification scale ($M_{GUT} \simeq 2 \times 10^{16}$ GeV). Assuming R-parity conservation, a specially attractive feature of the MSSM is the presence of the stable, weakly interacting lightest supersymmetric particle (LSP) in the form of lightest neutralino (χ_1^0) [2] which turns out to be a good candidate for the observed cold dark matter (CDM) in the universe.

However, the MSSM has a large number of soft breaking parameters, which make it less predictive in its most general forms. Most of these parameters can be elliminated by considering a definite SUSY breaking framework at the high scale. The simplest model in this regard, which assumes gravity as the mediator for SUSY breaking - the minimal supergravity (mSUGRA) [3] model - has only five free parameters. These are the common gaugino and scalar mass parameters $m_{1/2}$ and m_0, the common tri-linear coupling parameter A_0, all given at the gauge coupling unification scale, the ratio of Higgs vacuum expectation values at the electroweak scale, namely $\tan\beta$, and the sign of the Higgsino mixing parameter μ. The lightest neutralino can be expressed in terms of its gauge eigenstates, the Bino, the Wino and the two Higgsinos as

$$\chi_1^0 \equiv N_{11}\tilde{B} + N_{12}\tilde{W} + N_{13}\tilde{H}_D + N_{14}\tilde{H}_U. \tag{1}$$

The model is primarily associated with a Bino-dominated LSP that leads to over-abundance of dark matter. Reduction of the relic density to satisfy the WMAP data can be achieved if i) there is coannihilation of the LSP with another sfermion (usually stau $\tilde{\tau}_1$ or rarely $\tilde{t}_1$) that has a mass close to the mass of the LSP [4], ii) there is appropriate mixture of Bino and Higgsinos in the composition of the LSP so that there may be coannihalating charginos in the LSP-$\tilde{\chi}_1^{\pm}$ annihilation [5, 6] (the $\chi_1^0\chi_1^0 Z$ coupling is also enhanced), the so called focus point (FP) [7]/hyperbolic branch (HB) [8] region (this kind of coannihilation becomes significant when the LSP is dominantly Higgsino like), iii) the LSP is sufficiently small in mass and sfermions are light so that light sfermion exchange may enhance the LSP-LSP annihilation rates [1], or iv) there is a possibility of having s-channel Higgs exchanges occuring via the CP-odd Higgs boson A or via CP-even heavy (light) Higgs bosons H (h) leading to the "funnel region" of the dark matter satisfying zone in the $m_{1/2} - m_0$ plane [10, 11].

This simple model is highly predictive because of its small number of unknown parameters. However, a very severe restriction appears on the ($m_{1/2} - m_0$) plane of mSUGRA from the LEP2 bound on lightest Higgs boson mass (m_h) [12], which reads

$$m_h > 114.4 \text{ GeV}. \tag{2}$$

---

[1] This region known as *bulk annihilation* region, though highly constrained by the LEP2 limits on the Higgs boson mass, could be revived with non-vanishing A_0 parameter [9].

In order to satisfy the limit m_h >114 GeV within the framework of mSUGRA, one requires reasonably large values for the top squark mass ($\gg M_Z$) which implies some fine-tuning of SUSY parameters to obtain the correct value of M_Z. However, the limit of Eq.(2) is related to the principle Higgs search channel in the LEP2 that involves production of the Higgs boson via the $e^+e^- \to Zh$ process, followed by decays of the Higgs boson. The production process principally depends on the coupling g_{ZZh}. Now, in the MSSM, the coupling g_{ZZh} is not identical with the respective coupling in the SM, it can rather be written as $\sin(\beta-\alpha)g^{SM}_{ZZh}$(For reviews see [13, 14]). Here, g^{SM}_{ZZh} represents the SM Higgs coupling to the Z boson. The prefactor $\sin(\beta-\alpha)$ appears due to the mixing of the CP-even Higgs bosons, where α is the mixing angle. In supersymmetric theories the limit of Eq.(2) refers to the scenarios where $\sin(\beta-\alpha) \sim 1$. This corresponds to the so-called *decoupling* zone for the Higgs boson where one finds $m_A^2 >> M_Z^2$. In fact this is true for most of the parameter points in mSUGRA. However, in the general MSSM the above prefactor may become much smaller. This opens up a supersymmetric parameter space associated with a Higgs mass smaller than the limit of Eq.(2) (For details see [14]). This is the *non decoupling* zone for the Higgs boson, where all Higgs masses may have comparable values $m_h \simeq m_H \simeq m_A \sim M_Z$ [15, 16, 17, 18, 19, 20, 21, 22]. An important virtue is that with this new window, a light Higgs mass with $m_h \sim (95-100)$ GeV could explain the slight excess of events of 2.3σ statistical significance [15] as reported by the LEP2 experiments [12]. Within this *non decoupling* zone it is possible to have a Higgs boson lighter than the Z boson [16, 17]. In this regime, the Higgs mass does not require large radiative corrections, thus could evade the little hierarchy problem [18].

This particular region, which has recently been named as '*Light Higgs Boson*' scenario or LHS [17, 19], is also interesting as it provides definite predictions. Since all Higgs states are light enough, they can be produced at the Large Hadron Collider (LHC) [17]. Interestingly, this region can also accommodate the WMAP data for the dark matter relic density [19]. However, realization of the *light Higgs boson* scenario is not possible in the most constrained model like mSUGRA. Scenarios like supergravity - inspired nonuniversal Higgs mass models (NUHM), where the Higgs mass square parameters may have different values at the scale M_{GUT} ($m^2_{H_U}(M_{GUT}), m^2_{H_D}(M_{GUT})$) from the other scalars [23, 24], may be useful in this regard. Similarly, this particular SUSY zone can be realized in a particular nonuniversal scalar mass model where third generation squarks and the two Higgs doublets may have vanishing values at the GUT scale [25].

In this work, adapting a NUHM framework, we try to explore this particular parameter space in the light of recent dark matter detection experiments. Moreover, our focus will be to compute the indirect detection rate, particularly where the mass of the lightest neutralino and Higgs bosons are reasonably small. We will try to find out the parameter space where the WMAP data is satisfied via the resonant annihilation into a CP-odd Higgs boson. This is interesting as then neutralino pair annihilations in our galaxy could produce detectable signals both in the antiproton and the gamma-ray channels. In fact, the part of the MSSM parameter space with light neutralino masses which is otherwise forbidden in models like mSUGRA, can completely be explored in the near future. The other WMAP - satisfying zones, as mentioned, cannot produce such large anti-proton/gamma ray signals (except the FP/HB zone where the Bino dominated LSP with sufficient Higgsino component could lead to large signals). Defining a measure for these observables, we examine the detection prospects for the parameter space in the ongoing as well as upcoming experiments.

Now, it is not surprising that the neutralino - nucleus spin-independent scattering cross-section σ^{SI}, which is dominated by t-channel Higgs exchange (h, H) could be very large in the present context. The cross-section reaches its maximum value in the *non decoupling* zone because of smaller mass values of the CP-even Higgs bosons. In fact this particular region may fall within the range of the exclusion limits as given by CDMS-II [26] or XENON100 [27]. However there exist considerable uncertainties in the computation of the above cross-section as well as the relevant experimental limits. The principle sources are related to (i) nuclear form factors, (ii) the WIMP - nucleon scattering cross-section (mainly concerning the strange quark content of the nucleon), (iii) the local dark matter density and (iv) the escape velocity of the WIMP. Considering all these uncertainties and particularly exploiting the uncertainty related to the strange quark content of the nucleon we will see that the predicted neutralino-nucleus scattering cross-section σ^{SI} may change significantly. These uncertainties render the question of exclusion of interesting regions of the parameter space related to dark matter phenomenology subtle to answer.

The paper is organized as follows. In Sec.2 we will primarily discuss the model and the low energy constraints which are relevant here. In Sec.3 we introduce the spin-independent neutralino-nucleus scattering cross-section for the LSP. Similarly, Sec.4 is devoted to the indirect detection of the LSP, primarily to the (i) gamma-ray and the (ii) anti-proton signal. We describe our results in Sec.5. In Sec.6 we provide estimates regarding the effect of the uncertainties in the computation of σ^{SI}. Finally we conclude in Sec.7.

2 The NUHM and low energy constraints

In this section, we describe the model parameters and the relevant low energy constraints. As mentioned in the introduction, we place ourselves in a supergravity framework with nonuniversal Higgs masses at the GUT scale. Thus, the model can be specified by the following parameters:

$$m_{1/2}, A_0, m_0, m^2_{H_U}(M_{GUT}), m^2_{H_D}(M_{GUT}), sign(\mu), \tan\beta. \tag{3}$$

Here, $m_{1/2}$ and A_0 represent universal values for the gaugino masses and the trilinear coupling parameters, while m_0 denotes universal masses for all scalars except the Higgs bosons at the GUT scale. In general, Higgs scalars can belong to different multiplets of a grand unified gauge group, thus may assume different values than the other scalars in the theory (see [28] for motivated constructions leading to specific nonuniversal Higgs mass terms). In this spirit, we scan over the Higgs mass square parameters $m^2_{H_U}(M_{GUT})$ and $m^2_{H_D}(M_{GUT})$ at the scale M_{GUT} to produce a MSSM parameter space consistent with all low energy constraints and where Higgs bosons can be reasonably lighter. Using the Renormalization Group Equations (RGE) for the soft SUSY breaking parameters along with the conditions for radiative EWSB one can determine μ and m_A through

$$\mu^2 = -\frac{1}{2}M_Z^2 + \frac{m^2_{H_D} - m^2_{H_U}\tan^2\beta}{\tan^2\beta - 1} + \frac{\Sigma_1 - \Sigma_2\tan^2\beta}{\tan^2\beta - 1} \tag{4}$$

and

$$\sin 2\beta = 2B\mu/(m_{H_D}^2 + m_{H_U}^2 + 2\mu^2 + \Sigma_1 + \Sigma_2) \tag{5}$$

where the Σ_i's represent the one-loop corrections [29, 30], which become small at the scale where the Higgs potential V_{Higgs} is minimized. We can approximate $\mu^2 \sim -m_{H_U}^2$ (for $\tan\beta \geq 5$) and $m_A^2 = m_{H_D}^2 + m_{H_U}^2 + 2\mu^2 \sim m_{H_D}^2 - m_{H_U}^2$ at tree level. The parameters μ and the sparticle spectrum have been computed with SuSpect [31]. We consider the following collider constraints in addition to the bounds on sparticle masses [32] :

- **Higgs boson mass limit:** In the *non decoupling* region where the A boson becomes very light so that one has $m_A \sim m_H \sim m_h \sim M_Z$, the lower limit of m_h goes down to 93 GeV or even lower. We consider that the parameter space with $\sin^2(\beta - \alpha) < 0.3$ (or, $\sin(\beta - \alpha) < 0.55$), but with Higgs mass $93 < m_h < 114$ is in agreement with the LEP2 limit [12]. In practice, relaxing the constraint marginally we discern this zone with a value $\sin(\beta - \alpha) < 0.6$. Consequently, the coupling of the heavier Higgs boson to the Z boson ($g_{ZZH} \propto \cos(\beta - \alpha)$) becomes dominant and this makes the heavier Higgs boson SM - like ($\cos(\beta - \alpha) \sim 1$) with the same lower bound as in Eq.(2). In summary, to obtain acceptable SUSY spectra with $93 < m_h < 114$, in addition to the desired value for $\sin(\beta - \alpha)$, one also requires $m_H > 114$ GeV.

  On the other hand, in the decoupling region ($\sin(\beta - \alpha) \sim 1$), the limit of Eq.(2) needs to be respected. However we note that there is an uncertainty of about 3 GeV in computing the mass of the light Higgs boson [33]. This theoretical uncertainty primarily originates from momentum-independent as well as momentum-dependent two-loop corrections and higher loop corrections from the top-stop sector. Consequently, a lower limit of 111 GeV is often accepted for the SUSY light Higgs boson mass.

- $Br(b \to s\gamma)$ **constraint:** The most significant contributions to $b \to s\gamma$ originate from charged Higgs and chargino exchange diagrams in models like mSUGRA. The charged Higgs (H^--t loop) contribution has the same sign and comparable strength with respect to the W^--t loop contribution of the SM, which already saturates the experimental result. Hence, in scenarios where the charged Higgs mass can be very small, satisfying the $b \to s\gamma$ constraint requires a cancellation between the charged Higgs and the chargino exchange diagrams. We will choose A_0 such that most of the parameter points, especially WMAP - compliant ones, can satisfy this constraint. The effect of this constraint in the *light Higgs boson* zone has been discussed in [18]. We have used the following 3σ level constraint from $b \to s\gamma$ with the following limits [34].

  $$2.77 \times 10^{-4} < Br(b \to s\gamma) < 4.33 \times 10^{-4}. \tag{6}$$

- $Br(B_s \to \mu^+\mu^-)$ **constraint:** Similarly, the flavor physics observable $B_s \to \mu^+\mu^-$ may become very significant in this particular parameter space. The current experimental limit for $Br(B_s \to \mu^+\mu^-)$ coming from CDF [35] can be written as (at 95 % C.L.)

$$\mathrm{Br}(B_s \to \mu^+\mu^-) < 5.8 \times 10^{-8}, \tag{7}$$

which has recently been improved to $< 4.3 \times 10^{-8}$ at 95% C.L [36]. The estimate of $B_s \to \mu^+\mu^-$ in the MSSM depends strongly on the mass of A-boson and on the value of $\tan\beta$. In particular, the neutral Higgs boson contribution scales as m_A^{-4} whereas there is a $(\tan\beta)^6$ type of dependence. However, in the present analysis, we choose $\tan\beta$ (= 10) which makes this constraint less restrictive for most of the parameter space.

- **WMAP constraint :** In computing the relic density constraint, we consider the following 3σ limit of the WMAP data [37],

$$0.091 < \Omega_{CDM}h^2 < 0.128. \tag{8}$$

Here $\Omega_{CDM}h^2$ is the dark matter relic density in units of the critical density and $h = 0.71 \pm 0.026$ is the Hubble constant in units of 100 Km s^{-1} Mpc^{-1}. We use the code micrOMEGAS [38] to compute the neutralino relic density.

3 Direct Detection of Dark Matter

Direct detection of the LSPs involves measurement of recoil energies of nuclei as they are scattered by WIMPs. The effective Lagrangian that describes $\chi_1^0 - q$ elastic scattering at small velocities is given by (for reviews see [39])

$$\mathcal{L} = \alpha'_{qi}\bar{\chi}_1^0\gamma^\mu\gamma^5\chi_1^0\bar{q}_i\gamma_\mu\gamma^5 q_i + \alpha_{qi}\bar{\chi}_1^0\chi_1^0\bar{q}_i q_i \ . \tag{9}$$

The first term represents spin-dependent scattering while the second term refers to spin-independent scattering. Eq.(9) assumes summing over both the quark generations q while the subscript i runs for up ($i = 1$) and down type ($i = 2$) quarks respectively. The neutralino-quark coupling coefficients α_q and α'_q contain all SUSY model-dependent information. The spin-independent scattering cross-section of a neutralino with a target nucleus of proton number (atomic number) Z and neutron number $A - Z$ (A being the mass number) is given by

$$\sigma^{SI} = \frac{4m_r^2}{\pi}\left[Zf_p + (A-Z)f_n\right]^2 \ . \tag{10}$$

Where m_r is the reduced mass defined by $m_r = \frac{m_{\chi_1^0}m_N}{(m_{\chi_1^0}+m_N)}$ and m_N refers to the mass of the nucleus. The quantities f_p and f_n contain all the information of short-distance physics and nuclear partonic strengths. These are given by

$$\frac{f_{p,(n)}}{m_{p,(n)}} = \sum_{q=u,d,s} f_{Tq}^{(p,(n))}\frac{\alpha_q}{m_q} + \frac{2}{27}f_{TG}^{(p,(n))}\sum_{c,b,t}\frac{\alpha_q}{m_q} \ , \tag{11}$$

where $f_{Tq}^{(p,(n))}$ defined as

$$m_{p,(n)} f_{Tq}^{(p,(n))} = \langle p,(n)|m_q \bar{q} q|p,(n)\rangle \equiv m_q B_q \ . \tag{12}$$

The quantities $f_{Tq}^{(p,(n))}$ can be evaluated using a few hadronic data [40]. The gluon - related part namely $f_{TG}^{(p,(n))}$ is given by

$$f_{TG}^{(p,(n))} = 1 - \sum_{q=u,d,s} f_{Tq}^{(p,(n))} \ . \tag{13}$$

The numerical values of $f_{Tq}^{(p,(n))}$ may be seen in [40, 41]. We compute the neutralino-nucleon spin-independent scattering cross-section by using the code DarkSusy [42]. We should note here that the parameter $f_{Ts}^{(p,(n))}$ requires the information of the pion-nucleon sigma term $\sigma_{\pi N}$ and the size of the $SU(3)$ symmetry breaking-σ_0 as $f_{Ts}^{(p,(n))} \propto (\sigma_{\pi N} - \sigma_0)$, so that the leading contribution in σ^{SI} goes as $\sim (\sigma_{\pi N} - \sigma_0)^2$. Clearly, uncertainty in the computation of $\sigma_{\pi N}$ can produce significant shift to the strange quark parameter $f_{Ts}^{(p,(n))}$ and consequently to the measured spin-independent cross-section. Recent lattice results hint towards much smaller values of the $f_{Ts}^{(p,(n))} \sim 0.02$ [20, 43], a value much smaller than previous estimates. Considering even larger uncertainty in $\sigma_{\pi N}$ one may assume $\sigma_{\pi N} = \sigma_0$ which leads to $f_{Ts}^{(p,(n))} = 0$ [44]. In DarkSusy [42] the above coefficient is chosen as $f_{Ts}^{(p,(n))} \equiv 0.14$. This could provide a significant change in the results of the σ^{SI}. In fact, in [20, 44], the variation in the spin-independent cross-section due to this reduced $f_{Ts}^{(p,(n))}$ has been estimated. We shall also compute the variation in the spin-independent cross-section with the reduced values of $f_{Ts}^{(p,(n))}$. Similarly, we shall comment on the other sources of uncertainties and consequently their effects on σ^{SI} and the corresponding experimental limits.

The scalar cross-section depends on t-channel Higgs exchange (h, H) and s-channel squark exchange diagrams ($\sigma^{SI} \sim \frac{1}{m^4_{H,h,\tilde{q}}}$). Now, considering the strong bounds on the light squark masses, σ^{SI} is dominated by the exchange of CP-even Higgs bosons. In the present context, where both CP-even Higgs masses are quite small, σ^{SI} becomes enhanced. In fact, we shall see that in the mass range $93 < m_h < 114$, the spin-independent cross-section becomes maximal and this renders the *light Higgs boson* zone highly constrained even for $\tan\beta = 10$. Apart from the masses of the Higgs bosons, the cross-section depends strongly on the couplings $\chi_1^0 \chi_1^0 h(H)$ ($\mathcal{C}_{\chi_1^0 \chi_1^0 h(H)}$) and also on $h(H) q\bar{q}$ ($\mathcal{C}_{q\bar{q}h(H)}$). The latter contributions in the context of down - type fermions include $\tan\beta$ as $\mathcal{C}_{q\bar{q}h} \sim \tan\beta \cos(\beta - \alpha)$ and $\mathcal{C}_{q\bar{q}H} \sim \tan\beta \sin(\beta - \alpha)$. Clearly, both couplings may become quite large for larger values of $\tan\beta$. These large couplings, in addition to the small mass values for $m_{h,H}$, make this *light Higgs boson* zone almost ruled out for larger values of $\tan\beta$.

4 Indirect Detection of Dark Matter

Indirect detection techniques are based on the detection of primary or secondary particles resulting from dark matter (DM) annihilation or decay. The observed flux of these particles is proportional to the annihilation rate of the DM species which in turn is, for the annihilating case, proportional to ρ^2, the dark matter density profile. In the following, we summarize the basic ingredients of the formalism that we shall be employing in this work.

4.1 Gamma-ray Detection

4.1.1 The flux at intermediate latitudes

The differential flux of gamma–rays generated from dark matter annihilations and coming from a direction forming an angle ψ with respect to the galactic center (GC) is

$$\frac{d\Phi}{dE}(\psi, E) = N \frac{1}{4\pi} \frac{\langle \sigma v \rangle}{m_\chi^2} \sum_f \frac{dN_f}{dE} \int_{los} \rho^2(l(\psi)) dl(\psi), \tag{14}$$

where $N = 1, 1/2$ if the annihilating particle is Majorana-like or Dirac-like respectively, $\langle \sigma v \rangle$ is the total self annihilation cross-section averaged over velocity for $v \to 0$, m_χ is the mass of any DM particle , dN_f/dE is the differential spectrum of final state f into gamma-rays of energy E and ρ is the dark matter density profile. We note that in this work we only focus on prompt photons, ignoring potential contributions from synchrotron emission or inverse Compton scattering of charged particles with the interstellar medium.

The functions $\frac{dN_f}{dE}$ have been computed using the fragmentation of Standard Model particles into γ-rays according to the PYTHIA [45] Monte Carlo code.

Now, of course, we don't observe annihilations along a line but rather within a conical region around some angle ψ_0. It is convenient to define the dimensionless quantity

$$J(\psi) = \frac{1}{R_0} \frac{1}{\rho_0^2} \int_{los} \rho^2(l(\psi)) dl(\psi), \tag{15}$$

where R_0 is the sun's distance from the galactic center and ρ_0 the local DM density (actually, they can be any arbitrary normalization factors rendering J a dimensionless quantity).
Then, we can define the average of this quantity within a solid angle $\Delta\Omega$ as

$$\bar{J}(\Delta\Omega, \psi_0) = \frac{1}{\Delta\Omega} \int_{\Delta\Omega(\psi_0)} J(\psi) d\Omega, \tag{16}$$

and we can then rewrite the flux as

$$\frac{d\Phi}{dE}(\psi, E) = \frac{N}{4\pi} \frac{\langle \sigma v \rangle}{m_\chi^2} \left(\sum_f \frac{dN_f}{dE} \right) R_0 \rho_0^2 \ \bar{J}(\Delta\Omega, \psi_0). \tag{17}$$

The most common region of the sky that is examined in the literature as a source of γ-rays is the galactic center, since it is the region where N-body simulations predict a maximization of the dark matter density distribution and, hence, the corresponding gamma-ray flux. However, the galactic center is a region which is known poorly : There are large uncertainties in the background modelizations as well as the density profile itsself.

As an alternative, it has been proposed (see, for example, ref. [46]) that one could maximize the signal/background ratio by actually excluding the region around the galactic center. Following

	a [kpc]	α	β	γ	$\bar{J}$
Einasto	-	-		-	10.486
NFW	20	1.0	3.0	1.0	8.638
NFW$_c$	20	0.8	2.7	1.45	12.880

Table 1: Einasto, NFW and NFW$_c$ density profiles with the corresponding parameters, and values of $\bar{J}(\Delta\Omega)$ for the galactic region under consideration.

this reference, we perform our computations in a conoidal region extending from 20° up to 35° from the galactic center, excluding at the same time the regions within 10° from the galactic plane. It has actually been shown that within the framework of such an analysis, one can enhance the signal/background ratio by up to roughly an order of magnitude. The relevant background for this region will be discussed in the next subsection. It should also be noted that other regions of the sky might provide very interesting results, as shown for example in [47].

In the meantime, we present in table 1 the values obtained for the $\bar{J}$ quantity defined in eq.(16), for three different halo profiles often discussed in the literature: The Navarro, Frenck and White one (NFW) [48], which seems to be favoured by the recent results of the Via Lactea II simulation [49], the Einasto profile which is favoured by the findings of the Acquarius Project collaboration [50] and a NFW-like profile that has tried to take into account the effects of baryons in the inner galactic regions, causing an adiabatic collapse of DM in this area and a significant enhancement of its central density [51].

The $\bar{J}$ values obtained in the table demonstrate another virtue of searching for dark matter at intermediate latitudes, namely the fact that the results become quite robust with respect to the various dark matter density distribution modelizations. In the case of the galactic center, there can be differences of orders of magnitude in this factor, whereas in this case the differences are of $O(1)$. In the following, we shall be presenting our results for an Einasto profile, since it yields results somewhere in the middle among the other two scenarios.

4.1.2 The Fermi 1-year observations

The Fermi collaboration has published its 1-year observation results outside the GC [52]. In this paper, the collaboration presents its observations for a period of 19Msec and for various galactic latitudes. In the companion paper, the results for latitudes $20° < b < 60°$ are also presented, which lie actually in our region of interest. The data between $b = 10°$ and $20°$ are included in the same paper, presenting an enhancement by a factor of roughly $1.5 - 2$ with respect to the higher latitude data. In this analysis, for the sake of simplicity, we shall be focusing on the data from higher latitudes ($20° < b < 60°$), integrating them over the whole region of interest. This is justified, since we have excluded from our analysis the region within 20° from the galactic center, which should provide one of the major contributions to this spectrum.

In the paper, the authors could fit the data quite well using a Diffuse Galactic Emission model based on the GALPROP code. We find this model to be well reproduced, in our region of interest, by a simple power-law

$$\Phi_{\rm bkg}^{\rm Th} = 2.757 \cdot 10^{-6} E^{-2.49} \tag{18}$$

in units of GeV^{-1} sec^{-1} cm^{-2} sr^{-1}. In the same analysis, the collaboration presents the detector effective area values that should be used in order to compare predictions with observations, as a function of the gamma-ray energy. In the following, we shall be using these values rather than the usual nominal effective area of 10000 cm^2.

4.2 Antiproton Detection

Here, the charged particles present the complication of propagating throughout the Interstellar Medium (ISM) compared to the gamma-ray detection. Efforts have been made to describe the physics behind cosmic-ray propagation. Different treatments make different sets of assumptions and utilise different formalisms under specific assumptions [53, 54, 55, 56, 57, 58, 59]. Such treatments have of course been applied in the case of the MSSM neutralino dark matter detection [60, 61, 62, 63].

In this work, we shall use the two-zone diffusion model and its semi-analytical solution as described, for example, in references [57, 59]. In this model, positron and antiproton propagation takes place in a cylindrical region (Diffusive Zone, DZ) around the galactic center of half thickness L. Cosmic rays can escape this region, a case in which they are simply lost.

The master equation for cosmic-ray propagation is a diffusion-convection-reacceleration equation:

$$\partial_t \psi + \partial_z (V_c\, \psi) - \nabla (K\, \nabla \psi) - \partial_E \left[b(E)\, \psi + K_{EE}(E)\, \partial_E\, \psi \right] = q\,, \tag{19}$$

where $\psi = dn/dE$ is the space-energy density of the positrons or antiprotons, $b(E)$ is the energy loss rate, q is the source term, $V_c \approx (5-15)$ km/s is the convective wind velocity wiping away the positrons or antiprotons from the galactic plane,

$$K(E) = K_0\, \beta \left(\frac{E}{E_0} \right)^{\alpha} \tag{20}$$

is the diffusion coefficient, with β being the particle's velocity, K_0 the diffusion constant, α a constant slope, E the kinetic energy (for positrons in practice the total one), E_0 a reference energy (which we take to be 1 GeV), and

$$K_{EE} = \frac{2}{9}\, V_a^2\, \frac{E^2\, \beta^4}{K(E)} \tag{21}$$

is a coefficient describing reacceleration processes.

4.2.1 Differential Event Rate

In antiproton propagation, all energy redistributions in the initial (injection) spectrum –energy losses, reacceleration, as well as 'tertiary' contributions (i.e., contributions from antiprotons produced upon inelastic scattering of other antiprotons with the interstellar medium) can be ignored.

The importance of these redistributions depends on the antiproton energy. For GeV energies, the results may deviate up to 50% from those obtained with the (more complete) Bessel function treatment[2]. But for energies around 10 GeV, the accuracy of the method improves dramatically, yielding essentially indistinguishable results at slightly higher energies. Considering that the $\bar{p}$ energy region begins at 10 GeV, we can safely use this simplified approach.

Let us denote $\Gamma_{\bar{p}}^{\rm ann} = \sum_{\rm ISM} n_{\rm ISM}\, v\, \sigma_{\bar{p}\ {\rm ISM}}^{\rm ann}$, the destruction rate of antiprotons in the interstellar medium, where ISM = H and He, $n_{\rm ISM}$ is the average number density of ISM in the galactic disk, v is the antiproton velocity and $\sigma_{\bar{p}\ {\rm ISM}}^{\rm ann}$ is the $\bar{p} -$ ISM annihilation cross-section. Implementing the aforementioned simplifications, the transport equation for a point source (which actually defines the propagator G) is:

$$\left[-K\,\nabla + V_c\,\frac{\partial}{\partial z} + 2\,h\,\Gamma_{\bar{p}}^{\rm ann}\,\delta(z)\right] G = \delta\left(\vec{r} - \vec{r'}\right)\,, \tag{22}$$

with $h = 100$ pc being the half-thickness of the galactic disc. In this equation, the origin of the coordinate system is taken to be the Galactic Center, whereas $r = |\vec{r}_\odot - \vec{r}|$ is the distance of a given point from the sun. The presence of the δ function in the LHS of eq.(22) reflects the fact that we work in the so-called "thin disk" approximation, where the size of the diffusive zone is considered to be much larger than the size where spallations can take place [64]. The antiproton propagator connecting the solar position and any point in the diffusive zone can then be written (in cylindrical coordinates) as

$$G_{\bar{p}}^{\odot}(r,z) = \frac{e^{-k_v\,z}}{2\pi\,K\,L}\sum_{n=0}^{\infty} c_n^{-1}\,K_0\left(r\sqrt{k_n^2 + k_v^2}\right)\sin(k_n\,L)\,\sin(k_n\,(L-z))\,, \tag{23}$$

where K_0 is a modified Bessel function of the second kind and

$$\begin{aligned} c_n &= 1 - \frac{\sin(k_nL)\cos(k_nL)}{k_nL}\,, && (24)\\ k_v &= V_c/(2K)\,, && (25)\\ k_d &= 2\,h\,\Gamma_{\bar{p}}^{\rm ann}/K + 2\,k_v\,. && (26) \end{aligned}$$

k_n is obtained as the solution of the equation

$$n\,\pi - k_n\,L - \arctan(2\,k_n/k_d) = 0, \quad n \in \mathbb{N}\,. \tag{27}$$

Then, in order to compute the flux expected on earth, we should convolute the Green function (23) with the source distribution $q(\vec{x}, E)$. For the dark matter annihilations in the galactic halo, the source term is given by

$$q(\vec{x}, E) = \frac{1}{2}\left(\frac{\rho(\vec{x})}{m_\chi}\right)^2 \sum_i \left(\langle\sigma v\rangle\frac{dN_{\bar{p}}^i}{dE_{\bar{p}}}\right)\,, \tag{28}$$

where the index i runs over all possible annihilation final states. The decay and hadronization of SM particles into antiprotons are calculated with `PYTHIA` [45]. Now the distribution of dark matter

---

[2] In reference [57] a comparison between the two methods can be found (see figure 2).

	L [kpc]	K_0 [kpc^2/Myr]	α	V_c [km/s]
MIN	1	0.0016	0.85	13.5
MED	4	0.0112	0.70	12.0
MAX	15	0.0765	0.46	5.0

Table 2: Values of propagation parameters widely used in the literature and that provide minimal and maximal antiproton fluxes, or constitute the best fit to the B/C data.

in the Galaxy $\rho(\vec{x})$, is not the dominant factor in the calculation of the antiproton flux, thus we assume a standard NFW profile for the sake of definitiveness.
The antiproton flux on the earth can finally be expressed as

$$\Phi^{\bar{p}}_{\odot}(E_{\mathrm{kin}}) = \frac{c\,\beta}{4\pi}\frac{\langle\sigma v\rangle}{2}\left(\frac{\rho(\vec{x}_\odot)}{m_\chi}\right)^2 \frac{dN}{dE}(E_{\mathrm{kin}}) \int_{DZ} \left(\frac{\rho(\vec{x_s})}{\rho(\vec{x}_\odot)}\right)^2 G^{\odot}_{\bar{p}}(\vec{x}_s)\, d^3x_s \,. \tag{29}$$

Notice that since we ignore energy redistributions, the production and detection energy are the same. We hence compute the integral in equation (29) only once for each value of the injection energy (which is the same as the detection energy) by means of a VEGAS Monte-Carlo algorithm and use its values throughout our parameter space scan.

Regarding the propagation parameters L, K_0, α, and V_c, we take their values from the well-established MIN, MAX and MED models –see table 2. The MIN and MAX models correspond to the minimal and maximal antiproton fluxes that are compatible with the B/C data. The MED model, on the other hand, corresponds to the parameters that best fit the B/C data.

4.2.2 The background and antiproton detection with AMS-02

AMS-02 [65] is expected to be able to measure antiproton fluxes with an average geometrical acceptance of 330 cm^2 sr and energy above 16 GeV and up to 300 GeV. As mentioned in paragraph 4.2.1, we stick to energies above 10 GeV in this analysis. Similarly, we consider a 3-year run and the mentioned energy range is divided into 20 logarithmically evenly spaced energy bins.

At the same time, the PAMELA collaboration have recently published its updated antiproton measurements in the kinetic energy range from 60 MeV up to 180 GeV [66]. The data acquisition period was 850 days and the results seem to be in good agreement with several theoretical predictions for secondary production. Model-independent constraints from this data have been discussed, for example, in [67].

Above 10 GeV, which is the region of interest in our case, the data can be well described by a simple power law

$$\Phi_{\text{ bkg}} = 5.323 \times 10^{-4} E^{-2.935} \;\; \mathrm{GeV}^{-1}\mathrm{sec}^{-1}\mathrm{sr}^{-1}\mathrm{cm}^{-2}. \tag{30}$$

5 Results and Discussion

5.1 Cold Dark Matter Constraint and Light Higgs Boson Scenario

We present our main results in Figs.1 and 2, where we depict the valid parameter space consistent with the WMAP constraint in the $m_{1/2} - m_A$ plane, while assuming a moderate value for $\tan\beta(=10)$. Let us first concentrate on Fig.1. In this case, the other parameters are (i) $m_0 = 600$ GeV, (ii) $A_0 = -1100$ GeV[3]. We have varied the mass parameters $m^2_{H_U}(M_{GUT})$ $(0 < m^2_{H_U}(M_{GUT}) < m_0^2)$ and $m^2_{H_D}(M_{GUT})$ $(-1.5m_0^2 < m^2_{H_D}(M_{GUT}) < -0.5m_0^2)$ to obtain light neutralino dark matter consistent with light Higgs masses ($m_{H,A} \leq 250$ GeV) at the electroweak scale. As mentioned in Sec.2, μ and m_A are the derived quantities which we have calculated using Eqs.(4) and (5).

We are particularly concerned about the *light Higgs boson* zones and this, in the present case, requires $m_{1/2}$ values ≤ 160 GeV. The lightest neutralino in the form of $\tilde{B}$ (with a non negligible $\tilde{H}$ component) produces the acceptable relic density and we represent this through red circles. We also show contours for the lightest Higgs mass (m_h) and $\sin(\beta - \alpha)$. All points in the parameter space with $\sin(\beta - \alpha) < 0.6$ are considered to belong to the *light Higgs boson* zone where the Higgs mass can evade the LEP2 limit due to the reduced coupling with the Z boson. On the other hand, admitting a 3 GeV uncertainty in the Higgs mass calculation, as mentioned, we delineate the regions corresponding to 111 GeV $< m_h <$ 114 GeV. With a smaller $m_{1/2}$ value, the WMAP - allowed region predicts lighter squarks as well as lighter gluinos.

There are two distinct regions in the parameter space satisfying the relic abundance constraint:

(a) The light Higgs pole annihilation region where neutralino annihilation produces an acceptable relic density via the s-channel exchange of a light Higgs boson. This particular region extends in the direction of m_A with gaugino mass value ~ 140 GeV. This zone, however, is highly constrained in the mSUGRA model if one respects the flavor physics constraints [11, 72]. The spin-independent cross-sections [72], on the other hand, could be compatible with the CDMS-II [26] limits.

(b) The second region is the funnel region where the annihilations are principally due to exchange of A and H bosons, with $2m_{\chi_1^0} \simeq m_A, m_H$. Like in mSUGRA, this WMAP - satisfying region in the NUHM is principally characterized by the pseudoscalar Higgs boson - mediated resonant annihilation. The exact or near-exact resonance regions have very large annihilation cross-sections resulting in a high degree of under-abundance of dark matter. In fact, acceptable relic density can be produced when the A-width is quite large and $2m_{\chi_1^0}$ can be appreciably away from the exact resonance zone. This is precisely the reason for the two branches of red circles that extend along the direction of $m_{1/2}$ in Fig.1.

As already mentioned in the introduction, our primary interest is related to the region where $\sin(\beta - \alpha) < 0.6$. A lightest neutralino with mass $55 < m_{\chi_1^0} < 65$ GeV falls in this particular category with the A boson playing the dominant role in the annihilation process. Now, apart from the mass of the A bosons, neutralino pair annihilation also depends on the coupling $\mathcal{C}_{\chi_1^0\chi_1^0 A}$ which goes as the product of the Bino and Higgsino components of the LSP (N_{11} and N_{13}, N_{14} respectively). We recall that the Higgsino components of the LSP are essentially determined by the

---

[3] We consider a top pole mass $m_t = 173.1$ GeV [71]. Similarly we choose $sign(\mu) > 0$ in this analysis.

μ parameter. For a relatively large μ (500 GeV $< \mu <$ 750 GeV, Fig.1), the Higgsino component is relatively small which essentially diminishes the coupling $\mathcal{C}_{\chi_1^0\chi_1^0 A}$. In this regime, one finds that light neutralinos with mass ($m_{\chi_1^0} \sim 55 - 65$ GeV) can satisfy the WMAP constraint in the *non-decoupling* zone (i.e. where $m_A \sim 100$ GeV). We shall also present a scenario where a reasonably heavier neutralino ($m_{\chi_1^0} \sim 100$ GeV) can pair-annihilate efficiently in the *non-decoupling* zone via the enhancement of the $\mathcal{C}_{\chi_1^0\chi_1^0 A}$ coupling. Now, as neutralino masses increase, the funnel region extends in the direction of larger m_A and the Higgs bosons fall into the decoupling region (see Fig.1). Interestingly, even this WMAP - satisfying zone does not require large values of gaugino masses. We will observe that this whole region can lead to large gamma-ray as well as antiproton signals in present or oncoming experiments.

Before presenting our results on indirect detection, we would like to point out the results of the flavor physics observables like $b \to s\gamma$ and $B_s \to \mu^+\mu^-$. Since we have chosen a rather moderate value for $\tan\beta$ $(= 10)$, the $B_s \to \mu^+\mu^-$ constraint is not quite stringent for the parameter space shown in Fig.1. On the other hand $Br(b \to s\gamma)$ constitutes a strong constraint particularly in the *non-decoupling* region where charged Higgs bosons can be very light. However, with large negative A_0 values (negative values for A_t at the electro-weak scale), one of the stop eigenstates becomes lighter due to large mixing and this provides a cancellation between charged Higgs and chargino induced diagrams. Choosing $A_0 = -1100$ GeV at M_{GUT}, almost all parameter points and more importantly the whole WMAP allowed region in the $m_{1/2} - m_A$ plane can comply with the constraint. Now, in regard to the gray regions (Fig.1) one observes that: (i) For $m_{1/2} \geq 135$ GeV parameter space points with m_A smaller than roughly 100 GeV are not compatible with the Higgs mass limit in the *non-decoupling* zone i.e., here one has $m_h < 93$ GeV, (ii) for $m_{1/2} \leq 135$ GeV, the gluino becomes lighter (we impose $m_{\tilde{g}} > 390$ GeV for a valid parameter space point [73]) and then very soon the chargino becomes too light with $m_{\chi_1^\pm} < 103.5$ GeV. We should note here that a light Higgs with mass $m_h \leq 93$ GeV may be allowed, but then $\sin(\beta - \alpha)$ needs to be further suppressed. This region is then further constrained and we did not consider it in our analysis.

As discussed, with the choice of parameters of Fig.1, the *light Higgs boson* region is confined only up to $m_{\chi_1^0} \sim 65$ GeV. Since the flavor constraint $b \to s\gamma$ is particularly prohibitive, one needs to tune the A_0 to obtain a WMAP satisfied region compatible with the constraints from flavor physics. In principle, one could scan over the 4d parameter space namely $m_{1/2}, m^2_{H_U}(M_{GUT}), m^2_{H_D}(M_{GUT}), A_0$ to search for the complete $m_{\chi_1^0}$ range in the *light Higgs boson* region. However, rather than attempting a full, but very CPU - consuming scan over this entire parameter space, we choose to restrict ourselves to the subregions of the MSSM parameter space where the lightest neutralino can be light or relatively heavier.

Passing to Fig.2, we now explore part of the MSSM parameter space where pair annihilation of relatively heavier neutralinos in the *light Higgs boson* zone can conform the WMAP data via A exchange. We will see that the $\gamma/\bar{P}$ signals for this subset of the MSSM parameter space, in addition to the previous results, can be very illustrative to draw some general conclusions for the A annihilation region, particularly in the context of the *light Higgs boson* zone. This could be attributed to the fact that the A-funnel region is characterized by large pair annihilation cross-sections (insensitive to the velocity of LSP). Now, for simplicity we fix m_0 at the very similar value $m_0 = 600$ GeV, while $A_0 = -1000$ GeV is chosen to make $b \to s\gamma$ less restrictive. Here, we set $m^2_{H_U}(M_{GUT})$ $(= 2.4m_0^2)$ and varied $m^2_{H_D}(M_{GUT})$ $(-0.3m_0^2 < m^2_{H_D}(M_{GUT}) < 0.1)$ with $m_{1/2}$ to obtain the WMAP-compatible regions for neutralinos. Our scan renders very small μ values $(150 < \mu < 300)$, consequently the LSP can have large Higgsino components. With the choice of the input parameters that we assumed in this case, we find that the $m_{1/2} < 250$ GeV region is not quite compatible with the chargino mass limit.

We can see from Fig.2 that $m_{1/2} \sim 300$ GeV corresponds to the *non-decoupling* zone for the Higgs boson. Clearly, the lightest neutralino ($m_{\chi_1^0} \sim 120$ GeV) is quite far from the resonance annihilation condition i.e., $2m_{\chi_1^0} \simeq m_A$, thus the pair annihilation process actually occurs via off-shell A boson exchange (large Higgsino component enhances the neutralino coupling to the Higgs boson). Similarly, Z bosons in the s-channel and particularly, neutralinos in the t channel could also contribute significantly in the annihilation precesses. Thus, compared to the previous case, where the $b\bar{b}$ final state has the maximum branching ratio, here several other final states involving the Higgs bosons $(Zh, ZH, W^{\pm}H^{\pm}, hA, HA, hh)$ open up. We should note that $m_{\chi_1^0}$ cannot be much larger as then the neutralino would be further away from the resonance condition, which in turn makes the pair annihilation via A-boson exchange less significant. Similarly, one requires large Higgsino components or small μ parameter to satisfy the WMAP data, which is not favoured in the light of recent results of the spin-independent neutralino-nucleon cross-section. Alike the previous case, here the WMAP satisfying zone is compatible with the $b \to s\gamma$ constraint.

5.2 Exclusion and Detectability

Before presenting our results for indirect detection, we should define the measure, in particular what we mean by "exclusion" and "detectability". In order to assess whether a parameter space point is excluded by current data from Fermi or PAMELA, we should have some estimate of the background spectra for both gamma-rays and antiprotons. Till the present day, and despite the remarkable efforts devoted to the subject, no such generally accepted estimate exists. However, and quite generically, we expect the background to be of a power law form $\Phi_{bkg} = aE^b$ in both channels.

Now, every flux measurement contains both background as well as (hopefully) signal events. For every parameter space point, we can compute the gamma-ray or antiproton fluxes as described previously. Then, each point shall be considered as excluded if there is no (a, b) combination (i.e. the generic power-law background) for which the sum of the signal and the background can provide a good fit to the data. Hence, we vary (a, b), compute the corresponding backgrounds and then subsequently add the signal contribution to check if there exists some background form for which this sum provides a sufficiently good fit to the data. If no such (a, b) can be found, the corresponding parameter space point can be considered as excluded. In practice, the criterion we demand is that the sum of the signal and the background should fall within the 95% CL error bars as given by the Fermi or PAMELA collaborations.

The method we follow in order to characterize a parameter space point as being detectable has the same philosophy: First, we need some estimate of what future data could look like. To satisfy the criterion, we adopt a power law background that is compatible with current measurements. In order to minimize the signal's significance, we choose this background at the upper 68% CL error bar of the Fermi or PAMELA experimental points. Then, for each parameter space point, we add the signal to this background, creating a set of pseudo-data that could appear in the future. As pointed out, the exact form of the background is in general unknown, but its general form is expected to be a power-law, we could look for deviations of the pseudo-data from such a behaviour. If it is impossible to find a power law form that fits this pseudo-data well enough, then the corresponding parameter space point is characterized as detectable. If such an (a, b) combination can be found, then the signal shall be indistinguishable from the background (unless some other measurements allow to constrain the viable (a, b) combination, a possibility that we do not consider here). The goodness-of-fit criterion, what we choose is based on the χ^2 quantity, which is defined as

$$\chi^2 = \sum_{i=1}^{\text{nbins}} \frac{(N_{\text{bkg}} - N_{\text{exp}})^2}{N_{\text{bkg}}}, \tag{31}$$

where nbins is the number of bins, taken to be 20 in both cases, N_{exp} is the pseudo-data, whereas N_{bkg} is the background-only number of events that we try to fit to the pseudo-data.

If the best fitting power-law has a χ^2 larger than 28.87 (our problem has $20 - 2 = 18$ degrees of freedom, since we are trying to fit 2 variables (a, b)), this means that there is no (background-only) power-law that can fit the pseudo-data. Hence, if $\chi^2 > 28.87$ the corresponding parameter space point is detectable, since the signal it generates is distinguishable from the background.

If we wish to sum up our method in "hypothesis testing" terms, we could say that in the case of exclusion we are testing a null hypothesis according to which existing data can be well-described by dark matter annihilations plus some background form. In the detectability case, the null hypothesis is that the pseudo-data (containing both signal and background) can be well fitted by a background only function.

5.3 Indirect Detection results

Our analysis shows that the current Fermi and PAMELA data do not impose any constraints on the parameter space, at least as far as the WMAP-compliant regions are concerned. From now on, we shall therefore stick to predictions concerning the detection perspectives as described in the previous paragraph.

In Fig.1, with the choice of parameters described earlier, we also plot the contours where the χ^2 between the background-only fit and the pseudo-data becomes equal to 28.87, a case in which the background-only hypothesis can be rejected at 95% CL and the corresponding parameter space points are thus detectable for the case $A_0 = -1100$ GeV. The WMAP compatible region within the contours D^{γ} or $D^{\bar{P}}_{Max}$ has $\chi^2 \geq 28.87$ and is, thus, detectable. We assume the Einasto profile and the MAX propagation model for gamma-rays and antiprotons respectively. The contours for gamma-rays are blue-dashed whereas for antiprotons violet-dotted-dashed. All parameter space

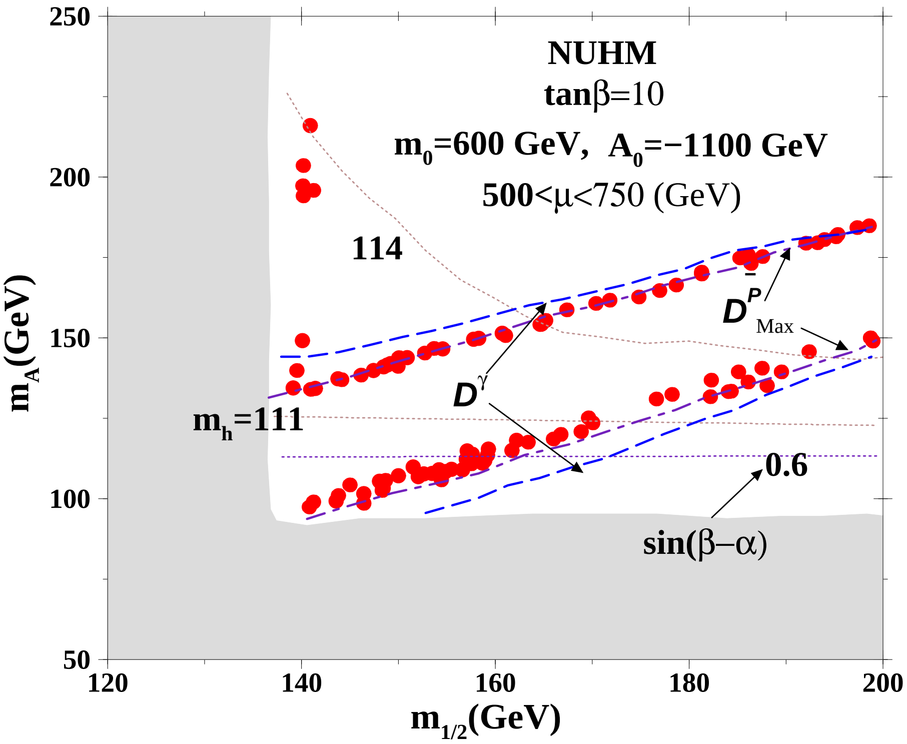

Figure 1: WMAP satisfied parameter points in the $m_{1/2} - m_A$ plane. Acceptable relic density is obtained via $s-$channel h, A or H exchange. Neutralino masses of $\sim 55-65$ GeV correspond to the *light Higgs boson* region. Detectability of the photon and anti-proton signal are represented by D^{γ} and $D^{\bar{p}}_{Max}$. The WMAP - compliant A pole annihilation region is within the reach of Fermi-GLAST and upcoming AMS-02 experiments.

points lying among the two lines which are quasi-symmetric around the resonnance are detectable according to our previous definitions.

We note that in the case of gamma-rays, switching to another profile does not significantly alter the results. In the case of antiprotons however, the results *do* change. For the sake of clarity we omit plotting these results, but we have calculated that both for the MIN and the MED propagation model defined previously and we find that some parts of the parameter space evade detection. We note that the points that satisfy WMAP through resonnant s - channel exchange of h persistently evade detection, a point on which we shall further comment in the following paragraphs.

Before explaining these results, we notice in [74] that, the Fermi satelite should in principle be able to exclude WIMPs with thermal cross-sections lying in our neutralino mass range and for $b\bar{b}$ final states. Furthermore, these estimates were extracted having in mind the Galactic Center as observation region. As mentioned, looking *around* this region can further improve the observation perspectives.

Concerning our results, it is interesting that practically all the points offer quite good detection perspectives. This is mainly related to the fact that the present values of the annihilation cross-

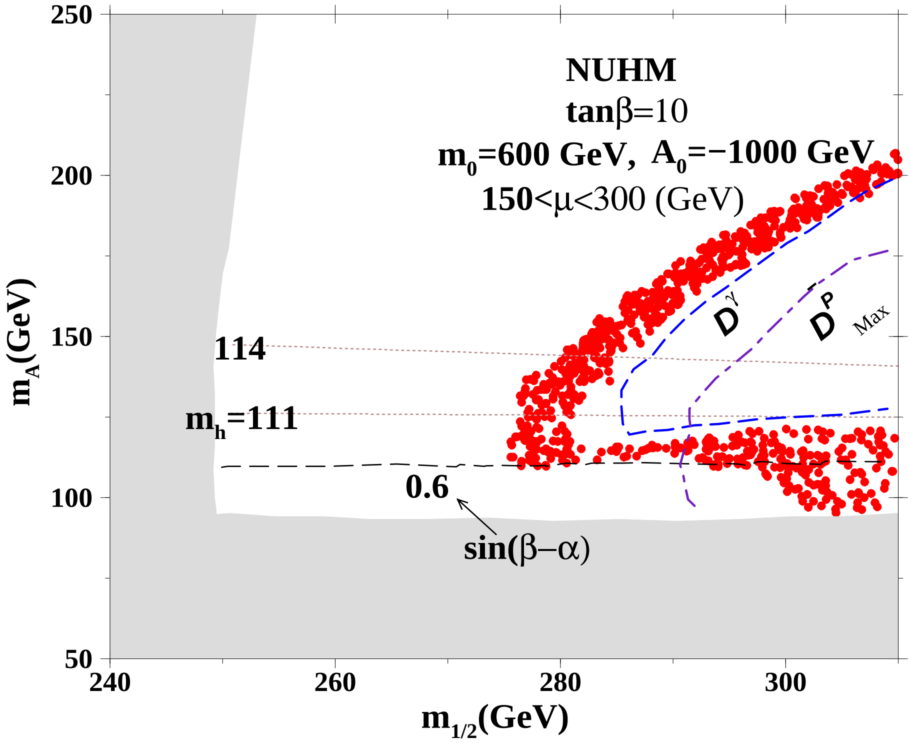

Figure 2: Same as Fig.1, except *light Higgs boson* zone is shifted to the larger values for neutralino masses.

sections for the parameter space points satisfying the WMAP constraints are quite high, namely of the same order as during the time of decoupling (i.e., in the thermal region). This is mainly due to the mechanism through which the correct relic density is actually obtained.

We already pointed out that in this scenario the mechanism that drives neutralino annihilation is resonnant s-channel pseudoscalar Higgs boson exhange, apart from the small region at low $m_{1/2}$ and relatively large m_A, where the dominant mechanism is CP-even light Higgs exchange. In the case of annihilation through an A propagator, the cross-section is practically insensitive to velocity changes as pointed out for example in [39]. This leads to the conclusion that the self-annihilation cross-section stays quite high even at present times. It is really instructive to compare this regime with the corresponding points where the acceptable relic density is produced via neutralino pair annihilation into h boson. In this case, $< \sigma v >$ tends to zero as the LSP velocity does so (i.e., at present times, which is relevant for indirect detection experiments).

This is indeed an interesting effect, which renders the h-pole points practically invisible to indirect detection experiments. The same has been pointed out, for example, in [75], where detectability limits (although defined differently) seem to systematically "avoid" the h-pole region. Now, we should note that the decay modes in the funnel region are dominated by the $b\bar{b}$ final states. This is due to the fact that neutralino pair annihilation into A and then into down type fermions is proportional to $\tan\beta$ along with the quark masses. It is well-known that the $(b\bar{b})$ final state yielding relatively rich photon spectra if compared, for example, to the leptonic case. On the other hand for the antiproton yield, the decays of light quarks have the tendency of producing more antiprotons than $b\bar{b}$ pairs.

Let us proceed to our second scenario, i.e., Fig.2. Once again, the blue-dashed line depicts region where $\chi^2 = 28.87$ for gamma-rays whereas the violet-dotted-dashed line represents the same condition for antiprotons. Astrophysical assumptions are the same as in the previous case. Points lying above, below or on the left of the contours are detectable. If we plotted the gamma-ray results for the other two profiles we examined, results would be practically unchanged. In the case of the two other propagation models for antiprotons, AMS-02 will be blind to the part of the relic density satisfying points. We can see that in this scenario, the perspectives are also quite good. We should note that we are still lying in the A-pole region (with significant contribution from $s-$channel Z and $t-$channel neutralino exchange): The neutralino annihilation is driven by the s-channel pseudoscalar exchange. Once again, $< \sigma v >$ lies roughly in the typical thermal region. But in this case, the lightest neutralino has a higher mass than previously. This is the reason why for relatively large values of $m_{1/2}$, we have a certain deterioration in the detection perspectives, particularly in the lower branch of the WMAP compliant parameter space. This is mostly visible in the antiproton channel, where we see that practically all LHS points are invisible at AMS-02. We have checked that if we consider more stringent gamma-ray detectability criterion, the same tendency would be visible for the corresponding contour as well. This behaviour could be connected to the fact that in this particular parameter space (lower branch), Higgs and gauge bosons have significant branching fraction in the final state. This is not the case for the upper branch, where the dominant channel is $b\bar{b}$. The main effect of a final state including Higgses is to shift the energy spectrum towards lower energies (since we consider the Higgs bosons to decay predominantly into $b\bar{b}$ pairs), where the background is larger. It is thus more difficult to disentangle the non-power law component of the spectrum (i.e. the signal) from the background.

In the two scenarios we examine two regimes, one with a quite light neutralino ($50 \lesssim m_{\chi_1^0} \lesssim 80$ GeV) and one with a relatively heavier one ($100 \lesssim m_{\chi_1^0} \lesssim 130$ GeV), finding that a good part of our parameter space should be visible at Fermi and AMS-02. There is, however, one question that could be asked, namely what happens in the intermediate mass regime, particularly in the context of *light Higgs boson* zone. The answer could be given once more by considering that it is well-known that increasing the WIMP mass tends to aggravate detection perspectives, if the same final states and self-annihilation cross-section are assumed. Both the Br_i's and $\langle\sigma v\rangle$ remain quite stable in value from lighter to higher masses in our model: The final state is mostly $b\bar{b}$ (in the second case Higgs final states are also significant which subsequently decays mostly into $b\bar{b}$) and the cross-section is of the typical thermal value, both during decoupling *and* at present times. Thus, it is easy to infer that the intermediate mass regime would also be able to produce rich $\gamma-$ray or anti-proton signals. Overall, this A-pole scenario that we have examined can be considered as quite promising for indirect detection. We shall further comment on that in the Conclusions section.

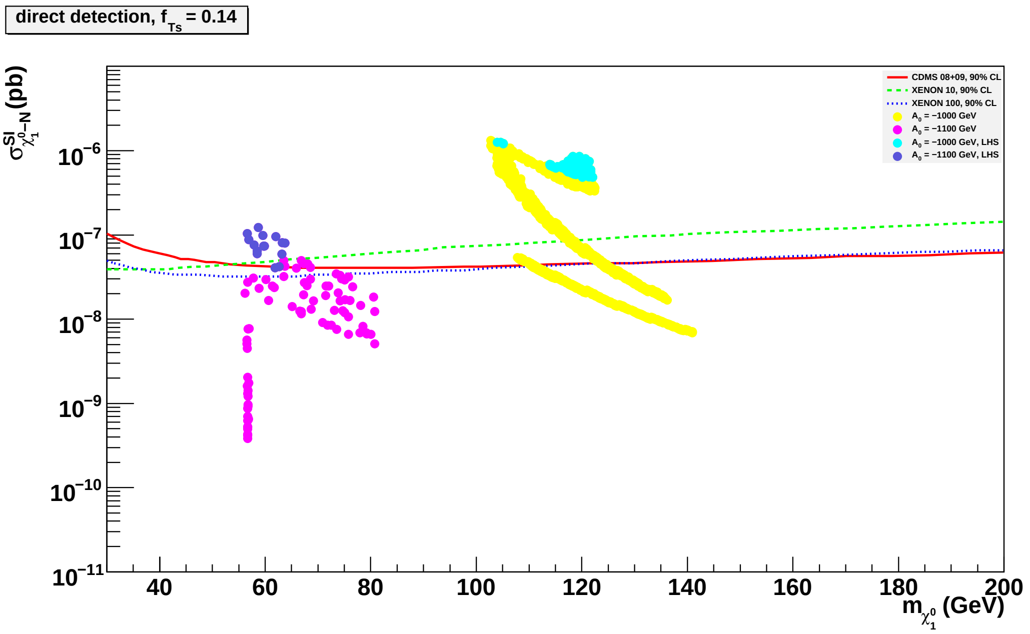

Figure 3: $(m_{\chi_1^0}, \sigma^{SI}_{\chi_1^0-N})$ combinations along with the relevant exclusion limits from direct detection experiments. The points lying above the lines are in principle excluded according to the published limits. Yellow points correspond to a trilinear coupling value of $A_0 = -1000$ GeV whereas pink ones to $A_0 = -1100$ GeV. The light blue and the dark blue points represent the *light Higgs boson* regime for the two scenarios respectively. $f^{(p,(n))}_{Ts}$ is taken at the default DarkSusy value, namely 0.14.

6 Discussion on the constraints from Direct Detection experiments

In Fig.3 we depict the WMAP-compliant parameter points on the $(m_{\chi_1^0}, \sigma^{SI}_{\chi_1^0-N})$ (neutralino mass - neutralino-nucleon spin-independent scattering cross-section) plane and compare them against the three strongest bounds available in the literature: The combined 2008 and 2009 CDMS-II [26] results, the constraints from the XENON10 experiment as well as the latest bounds from XENON100. We take the two former ones from ref. [76] and the latter from [27]. We further highlight the points falling into the light Higgs scenario defined throughout this paper with different colors.

We indeed see that many of our points fall largely within the region that is supposed to be excluded from the existing data. Whereas the $A_0 = -1100$ GeV scenario (pink points) is more or less satisfying the constraints, the scenario with $A_0 = -1000$ GeV (yellow points) is in most cases largely above the limits, exceeding by more than an order of magnitude compared to the CDMS-II and XENON100 allowed cross-sections. The large values for $\sigma^{SI}_{\chi_1^0-N}$ in the latter case can be attributed to the large Higgsino components of the neutralino which enhance the coupling $\mathcal{C}_{\chi_1^0\chi_1^0 h(H)}$. In both cases, the points belonging to the *light Higgs boson* region fall within the excluded zones.

However, it has been repeatedly pointed out in the literature that there can be significant uncertainties that complicate the assertion on whether a particular model is excluded or not [77]. More specifically:

- Uncertainties can arise in the calculation of the neutralino-nucleon elastic scattering cross-section, which can be due to a number of factors. For example, as described in detail in [44], significant uncertainties can arise in the passage from the parton-level cross-section to the hadronic level one.

- Some uncertainties might be present in the passage from the hadronic to the nuclear level. Indeed, at the end of the day the primarily constrained quantity is the WIMP-*nucleus* elastic scattering cross-section and not the WIMP-*nucleon* one.

- The local dark matter density is by no means a perfectly well known quantity and is in fact a normalization factor in the overall procedure of computing the WIMP-nucleus scattering rate. This uncertainty also enters in the indirect detection calculation, in fact in a more severe way since the gamma-ray or antiproton fluxes depend quadratically on the aforementioned quantity.

- Little is known on the true velocity distribution of the WIMPs in the detector rest frame as well as on the escape velocity at which the integral over the velocity distribution should be truncated.

The first point concerns our calculation of the spin-independent neutralino-nucleon elastic scattering cross-section. In other words, and refering to Fig.3, we expect that a certain variation in the position of parameter space points on the $(m_{\chi_1^0}, \sigma^{SI}_{\chi_1^0-N})$ plane should be allowed. The other remarks apply to the experimental limits published from the various collaborations, i.e., they can amount to a change in the position of the exclusion lines.

In ref. [44], a systematic study of the hadronic uncertainties entering the neutralino-nucleon scattering cross-section is performed. It turns out that the most striking and influential uncertainty comes from the pion-nucleon $\sigma_{\pi N}$ term which is poorly known but an essential ingredient for a precise calculation of the relevant cross-section. This source of uncertainty alone can give rise to a variation in the spin-independent cross-section of more than an order of magnitude [20, 44]. This means that the relevant neutralino-nucleon scattering cross-sections that we have calculated can in fact vary by a factor of more than 10. As mentioned in Sec.3, uncertainty in $\sigma_{\pi N}$ may decrease the coefficient $f_{Ts}^{(p,(n))}$ and this is in fact predicted by recent lattice simulation. Thus, we study the variation in $\sigma^{SI}_{\chi_1^0-N}$ with smaller $f_{Ts}^{(p,(n))}$ values. Following the discussion in Sec.3, here we consider two representative values for $f_{Ts}^{(p,(n))}$ namely 0.02 and 0. We present our results in fig.4. Indeed, we can see that the neutralino-nucleon spin-independent cross-sections decrease by significant factors, reaching up to an order of magnitude (particularly for $f_{Ts}^{(p,(n))} = 0$). This clearly starts raising questions on whether a good portion of the parameter space is excluded (as one would naively expect from Fig.3) or not.

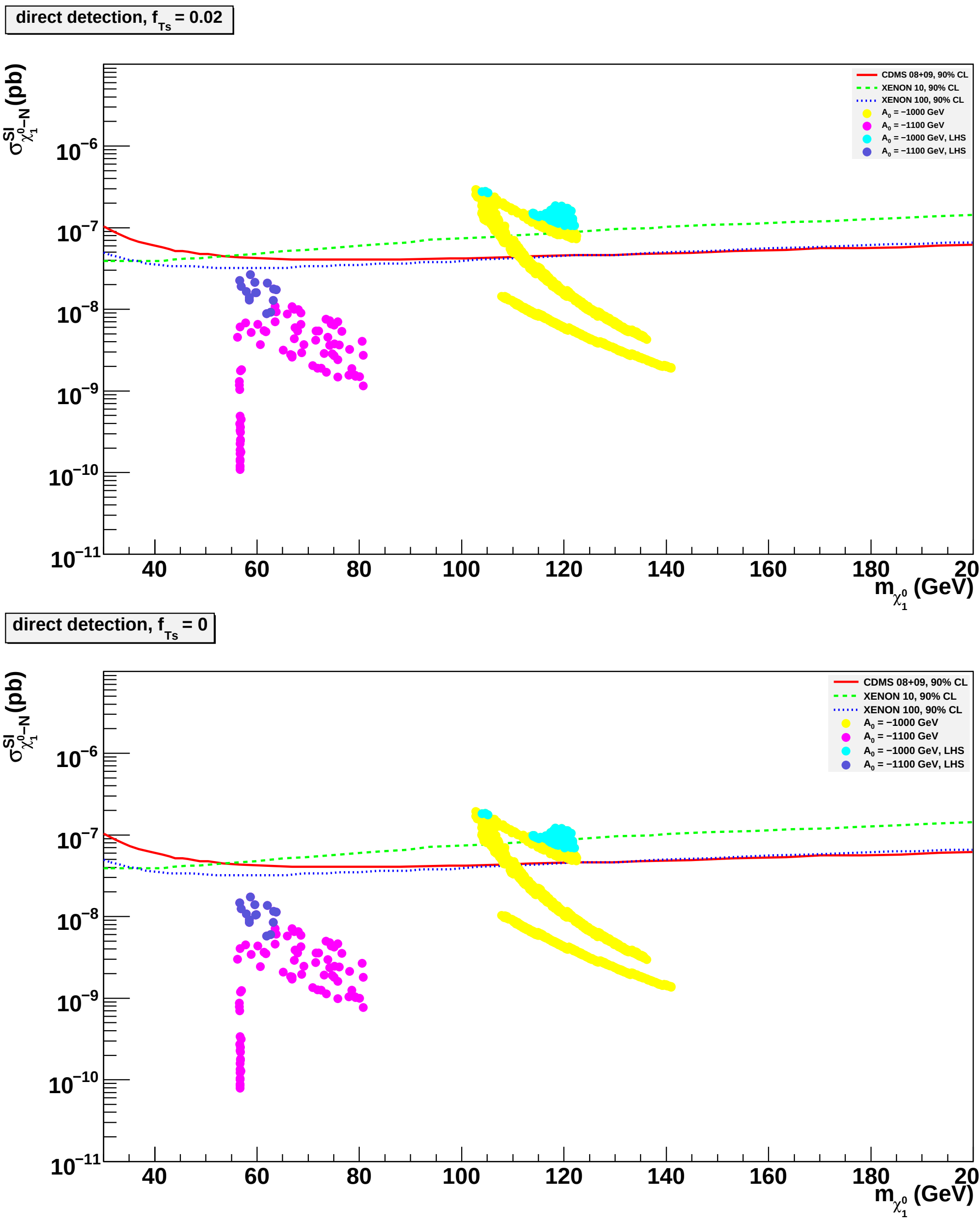

Figure 4: As in fig.3 but for $f_{Ts}^{(p,(n))} = 0.02$ (top) and 0 (bottom).

We see, however, that - especially in the heavier neutralino scenario - there are still some parameter points lying above the exclusion lines (roughly by a factor of $2-3$). This is particularly true for the LHS scenario. However, this conclusion may become weaker if one considers the other uncertainties which we describe below.

Passing to the nuclear level requires modelling of the nucleon density within the nucleus. The most commonly used parametrization is the one presented by Engel in [78]. Now, the deviation that might arise from different form factor parametrizations has been performed, for example, in [79], where the authors find that the exclusion lines can shift vertically by roughly a factor of 1.2.

Next, we discuss the uncertainty related to the local dark matter density. Most experimental analyses including the ones considered in the present work are performed assuming the so-called standard halo model. In this model, the local DM density is usually taken to have a fixed value of 0.3 GeV cm^{-3}. Typically, the uncertainties associated with the local density value are given to be of the order of $10\% - 20\%$ at a 68% confidence level, i.e., less than a factor of two. It is, however, true that these estimates depend on specific astrophysical assumptions. There have been authors who using a wide range of possible halo profiles [80] or no halo modelization at all [81] find values for the local density ranging from 0.2 up to roughly 0.5 GeV cm^{-3} at 68% CL. Furthermore, clumpy behaviour could further disrupt these estimates, although N-body simulations seem to rather disfavour such a possibility [82]. Thus there may be a factor ~ 2 variation in the local DM density, which would rescale the corresponding WIMP-nucleon scattering cross-section limits by the same amount.

A recent treatment of the astrophysical uncertainties involved in direct DM detection is [83], while a summary of some of these uncertainties with several references can also be found in [84]. Varying the escape velocity can play an important role either for larger LSP masses which are irrelevant in our case or for models involving quite different processes than the ones involved in the MSSM neutralino case [85]. The same applies to the uncertainties arising from the experimental error in the determination of the Sun's circular velocity around the galactic center, which assumes a Maxwell-Boltzmann velocity distribution for neutralinos. Therefore we expect only a small modifications in the exclusion limits ($\sim O(10\%)$) due to these aforementioned variations.

We see that overall, and despite the apparent exclusion of a large portion of LHS points, there is still quite some margin for changing the relation among the predicted $(m_{\chi_1^0}, \sigma^{SI}_{\chi_1^0-N})$ as derived from the model and the exclusion limits as presented by the corresponding collaborations. We feel it is reasonable to say that we cannot assess that easily whether the parameter space points lying above the exclusion lines in Fig.3 are actually excluded or not.

We should clarify at this point that the previous remarks have by no means the purpose of demeaning the remarkable works that are done both by theorists and experimentalists in order to develop tools for calculations and extract reliable bounds. Our goal was just to illustrate that it might still be meaningful to examine models which at first sight appear to be excluded. This becomes particularly apparent from our calculation of the spin-independent cross-section for different values of $f_{Ts}^{(p,(n))}$.

7 Conclusions

We have examined the dark matter - related phenomenology of a particular subset of the MSSM parameter space adapting nonuniversal Higgs masses at the GUT scale. We confine ourselves to a particular regime where the MSSM Higgs scalars as well as neutralinos can be relatively light. Our principal investigation is devoted where lightest CP-even Higgs boson is below the LEP2 limit, but still allowed due to the reduced value of ZZh coupling.

The WMAP limits on the dark matter relic density are satisfied by the neutralino self-annihilation through A, h or H propagators. For illustration purposes we have chosen two specific examples with different neutralino masses. Then we have examined the detectability of the scenarios in the current Fermi-LAT and the upcoming AMS-02 experiment for the detection of gamma-rays and antiprotons respectively.

We have found that overall the model offers quite promising detection prospects: The self-annihilation cross-section at zero velocity, relevant for indirect detection, is quite high, i.e., of the same order of magnitude as needed in order to get the correct relic density for the WIMPs. This is especially the case when annihilation is driven by s-channel pseudoscalar exchange. Furthermore, the final states being mostly comprised of $b\bar{b}$ pairs (with significant Higgs bosons final states for relatively larger neutralino masses), the resulting spectra are quite rich both in gamma-rays and antiprotons (especially for photons). In this context we did not consider the possibility of substructure in the galactic halo, which could enhance the signal by roughly a factor of 10 as is well-known in the literature.

Finally, we have computed the neutralino-nucleon spin-independent scattering cross-section and find that under the most common assumptions a significant part of the LHS region seems to be excluded by current direct detection measurements. We however showed that numerous uncertainties could severely influence this assessment.

Furthermore, the preceeding analysis demonstrates, once more, the value of a multi-messenger approach towards dark matter detection. Firstly, each detection mode offers a distinct probe for dark matter signals which can be used to cross-check others. Then, some regions of the parameter space might be undetectable in some channel, but visible in some other: This is the case of the LHS in our second benchmark, which is invisible in antiproton detection but visible in gamma-rays or direct detection. Overall, different detection techniques can act in a highly complementary way.

We would like to close this article with a remark that seems to have a more general validity than the model we examined in our case. As we said, the regions where the correct relic density can be obtained in the MSSM are quite limited in their general characteristics. One of them is the so-called funnel region, where the self-annihilation cross-section is enhanced through resonnant s - channel exchange of Higgses, h, H and A. In the latter case, it is known for quite some time that the cross-section does not depend strongly on the neutralino velocity. The fact that the Large Area Telescopes being at least as powerful as Fermi can probe self-annihilation cross-section values of the order of $3 \cdot 10^{-26}$ cm^3 sec and masses of roughly up to 200 GeV has also been demonstrated. It can hence be seen that the A - pole region for reasonable neutralino masses constitutes one of the most favoured regions for indirect detection in both the gamma-ray and the anti-proton channel. On the contrary, other WMAP compatible regions namely the h-pole resonance annihilation region or the coannihilation regions (where the Higgsino component is tiny) where the cross-section is much smaller at present times than during decoupling cannot produce so large indirect detection rates.

Acknowledgements

This work has been done partly under the ANR project TAPDMS No **ANR-09-JCJC-0146**. D.D. acknowledges support from the Groupement d'Intérêt Scientifique P2I. The work of AG and YM are supported in part by the E.C. Research Training Networks under contract **MRTN-CT-2006-035505**. The authors would like to thank the anonymous referee for valuable comments and remarks.

References

[1] For reviews on Supersymmetry, see, *eg*, H. P. Nilles, Phys. Rep. **1**, 110 (1984); H. E. Haber and G. Kane, Phys. Rep. **117**, 75 (1985) ; J. Wess and J. Bagger, *Supersymmetry and Supergravity*, 2nd ed., (Princeton, 1991); M. Drees, P. Roy and R. M. Godbole, *Theory and Phenomenology of Sparticles*, (World Scientific, Singapore, 2005); H. Baer and X. Tata, *Cambridge, UK: Univ. Pr. (2006) 537 p.*

[2] H. Goldberg, Phys. Rev. Lett. **50**, 1419 (1983); J. Ellis, J. Hagelin, D. Nanopoulos and M. Srednicki, Phys. Lett. **B127**, 233 (1983); J. Ellis, J. Hagelin, D. Nanopoulos, K. Olive and M. Srednicki, Nucl. Phys. **B238**, 453 (1984).

[3] A. H. Chamseddine, R. Arnowitt and P. Nath, Phys. Rev. Lett. **49**, 970 (1982); R. Barbieri, S. Ferrara and C. A. Savoy, Phys. Lett. B **119**, 343 (1982); L. J. Hall, J. Lykken and S. Weinberg, Phys. Rev. D **27**, 2359 (1983); P. Nath, R. Arnowitt and A. H. Chamseddine, Nucl. Phys. B **227**, 121 (1983); N. Ohta, Prog. Theor. Phys. **70**, 542 (1983); For reviews see [1] and P. Nath, R. Arnowitt and A.H. Chamseddine, *Applied N =1 Supergravity* (World Scientific, Singapore, 1984).

[4] J. R. Ellis, T. Falk and K. A. Olive, Phys. Lett. B **444**, 367 (1998); J. R. Ellis, T. Falk, K. A. Olive and M. Srednicki, Astropart. Phys. **13**, 181 (2000) [Erratum-ibid. **15**, 413 (2001)]; A. Lahanas, D. V. Nanopoulos and V. Spanos, Phys. Rev. D **62**, 023515 (2000); R. Arnowitt, B. Dutta and Y. Santoso, Nucl. Phys. B **606**, 59(2001); T. Nihei, L. Roszkowski and R. Ruiz de Austri, JHEP **0207**, 024 (2002); V. A. Bednyakov, H. V. Klapdor-Kleingrothaus and V. Gronewold, Phys. Rev. D **66**, 115005 (2002).

[5] J. Edsjo and P. Gondolo, Phys. Rev. D **56**, 1879 (1997).

[6] S. Mizuta and M. Yamaguchi, Phys. Lett. B **298**, 120 (1993).

[7] J. L. Feng, K. T. Matchev and T. Moroi, Phys. Rev. D **61**, 075005 (2000); Phys. Rev. Lett. **84**, 2322 (2000); J. L. Feng, K. T. Matchev and F. Wilczek, Phys. Lett. B **482**, 388 (2000); U. Chattopadhyay, A. Datta, A. Datta, A. Datta and D. P. Roy, Phys. Lett. B **493**, 127 (2000); U. Chattopadhyay, T. Ibrahim and D. P. Roy, Phys. Rev. D **64**, 013004 (2001); J. L. Feng and F. Wilczek, Phys. Lett. B **631**, 170 (2005); S. P. Das, A. Datta, M. Guchait, M. Maity and S. Mukherjee, Eur. Phys. J. C **54**, 645 (2008), [arXiv:0708.2048 [hep-ph]].

[8] K. L. Chan, U. Chattopadhyay and P. Nath, Phys. Rev. D **58**, 096004 (1998); U. Chattopadhyay, A. Corsetti and P. Nath, Phys. Rev. D **68**, 035005 (2003).

[9] U. Chattopadhyay, D. Das, A. Datta and S. Poddar, Phys. Rev. D **76**, 055008 (2007) [arXiv:0705.0921 [hep-ph]].

[10] M. Drees and M. Nojiri, Phys. Rev. **D47**, 376 (1993); R. Arnowitt and P. Nath, Phys. Rev. Lett. **70**, 3696 (1993); H. Baer and M. Brhlik, Phys. Rev. **D53**, 597 (1996), Phys. Rev. D **57**, 567 (1998); H. Baer, M. Brhlik, M. Diaz, J. Ferrandis, P. Mercadante, P. Quintana and X. Tata, Phys. Rev. **D63**, 015007 (2001); J. R. Ellis, T. Falk, G. Ganis, K. A. Olive and M. Srednicki, Phys. Lett. B **510**, 236 (2001); A. B. Lahanas and V. C. Spanos, Eur. Phys. J. **C23**, 185 (2002).

[11] A. Djouadi, M. Drees and J. L. Kneur, Phys. Lett. B **624**, 60 (2005).

[12] R. Barate *et al.* [LEP Working Group for Higgs boson searches], Phys. Lett. B **565**, 61 (2003) [arXiv:hep-ex/0306033].

[13] J. F. Gunion and H. E. Haber, Nucl. Phys. B **272**, 1 (1986) [Erratum-ibid. B **402**, 567 (1993)]; M. Carena and H.E. Haber, Prog. Part. Nucl. Phys. **50**(2003) 63.

[14] A. Djouadi, Phys. Rept. **459**, 1 (2008) [arXiv:hep-ph/0503173].

[15] M. Drees, Phys. Rev. D **71**, 115006 (2005) [arXiv:hep-ph/0502075].

[16] G. L. Kane, T. T. Wang, B. D. Nelson and L. T. Wang, Phys. Rev. D **71**, 035006 (2005) [arXiv:hep-ph/0407001].

[17] A. Belyaev, Q. H. Cao, D. Nomura, K. Tobe and C. P. Yuan, Phys. Rev. Lett. **100**, 061801 (2008) [arXiv:hep-ph/0609079].

[18] S. G. Kim, N. Maekawa, A. Matsuzaki, K. Sakurai, A. I. Sanda and T. Yoshikawa, Phys. Rev. D **74**, 115016 (2006) [arXiv:hep-ph/0609076].

[19] M. Asano, S. Matsumoto, M. Senami and H. Sugiyama, Phys. Lett. B **663**, 330 (2008) [arXiv:0711.3950 [hep-ph]]; M. Asano, S. Matsumoto, M. Senami and H. Sugiyama, arXiv:0912.5361 [hep-ph].

[20] J. Cao, K. i. Hikasa, W. Wang, J. M. Yang and L. X. Yu, arXiv:1006.4811 [hep-ph].

[21] E. Boos, A. Djouadi, M. Muhlleitner and A. Vologdin, Phys. Rev. D **66** 055004 (2002); E. Boos, A. Djouadi and A. Nikitenko, Phys. Lett. B **578**, 384 (2004); E. Boos, V.Bunichev, A. Djouadi and H.J. Schreiber, Phys. Lett. B **622** 311 (2005).

[22] A. Djouadi and Y. Mambrini, JHEP **0612**, 001 (2006).

[23] R. Rattazzi, U. Sarid and L. J. Hall, arXiv:hep-ph/9405313; N. Polonsky and A. Pomarol, Phys. Rev. Lett. **73**, 2292 (1994) [arXiv:hep-ph/9406224]; D. Matalliotakis and H. P. Nilles, Nucl. Phys. B **435**, 115 (1995) [arXiv:hep-ph/9407251]; N. Polonsky and A. Pomarol, Phys. Rev. D **51**, 6532 (1995) [arXiv:hep-ph/9410231].

[24] P. Nath and R. L. Arnowitt, Phys. Rev. D **56**, 2820 (1997) [arXiv:hep-ph/9701301]; J. R. Ellis, T. Falk, K. A. Olive and Y. Santoso, Nucl. Phys. B **652**, 259 (2003) [arXiv:hep-ph/0210205]; J. R. Ellis, K. A. Olive, Y. Santoso and V. C. Spanos, Phys. Lett. B **603**, 51 (2004); H. Baer, A. Mustafayev, S. Profumo, A. Belyaev and X. Tata, JHEP **0507**, 065 (2005); H. Baer, A. Mustafayev, S. Profumo, A. Belyaev and X. Tata, Phys. Rev. D **71**, 095008 (2005); J. R. Ellis, K. A. Olive and P. Sandick, Phys. Rev. D **78**, 075012 (2008); J. Ellis, K. A. Olive and P. Sandick, New J. Phys. **11**, 105015 (2009).

[25] U. Chattopadhyay and D. Das, Phys. Rev. D **79**, 035007 (2009) [arXiv:0809.4065 [hep-ph]]; S. Bhattacharya, U. Chattopadhyay, D. Choudhury, D. Das and B. Mukhopadhyaya, Phys. Rev. D **81**, 075009 (2010) [arXiv:0907.3428 [hep-ph]].

[26] Z. Ahmed *et al.* [The CDMS-II Collaboration], arXiv:0912.3592 [astro-ph.CO].

[27] E. Aprile *et al.* [XENON100 Collaboration], arXiv:1005.0380 [astro-ph.CO].

[28] L. Calibbi, Y. Mambrini and S. K. Vempati, JHEP **0709** (2007) 081 [arXiv:0704.3518 [hep-ph]]; L. L. Everett, I. W. Kim, P. Ouyang and K. M. Zurek, Phys. Rev. Lett. **101** (2008) 101803 [arXiv:0804.0592 [hep-ph]]. E. Dudas, Y. Mambrini, S. Pokorski, A. Romagnoni and M. Trapletti, JHEP **0903** (2009) 011 [arXiv:0809.5064 [hep-th]]; M. Holmes and B. D. Nelson, JCAP **0907** (2009) 019 [arXiv:0905.0674 [hep-ph]]; M. Endo, S. Shirai and K. Yonekura, JHEP **1003** (2010) 052 [arXiv:0912.4484 [hep-ph]].

[29] R. Arnowitt and P. Nath, Phys. Rev. D **46**, 3981 (1992).

[30] G. Gamberini, G. Ridolfi and F. Zwirner, Nucl. Phys. B **331**, 331 (1990); V. D. Barger, M. S. Berger and P. Ohmann, Phys. Rev. D **49**, 4908 (1994); For two-loop effective potential see: S. P. Martin, Phys. Rev. D **66**, 096001 (2002).

[31] A. Djouadi, J. L. Kneur and G. Moultaka, Comput. Phys. Commun. **176**, 426 (2007), [arXiv:hep-ph/0211331].

[32] For the latest limits on the sparticle masses from LEP experiments: see http://lepsusy.web.cern.ch/lepsusy/

[33] G. Degrassi, S. Heinemeyer, W. Hollik, P. Slavich and G. Weiglein, Eur. Phys. J. C **28**, 133 (2003); B. C. Allanach, A. Djouadi, J. L. Kneur, W. Porod and P. Slavich, JHEP **0409**, 044 (2004); S. Heinemeyer, W. Hollik and G. Weiglein, Phys. Rept. **425**, 265 (2006) [arXiv:hep-ph/0412214]; S. Heinemeyer, hep-ph/0408340; S. Heinemeyer, Int. J. Mod. Phys. A **21**, 2659 (2006).

[34] P. Koppenburg *et al.* [Belle Collaboration], Phys. Rev. Lett. **93**, 061803 (2004) B. Aubert, et al., BaBar Collaboration, hep-ex/0207076; E. Barberio *et al.* [Heavy Flavor Averaging Group (HFAG)], arXiv:hep-ex/0603003.

[35] T. Aaltonen *et al.* [CDF Collaboration], Phys. Rev. Lett. **100**, 101802 (2008).

[36] M. J. Morello [CDF Collaboration and D0 Collaboration], arXiv:0912.2446 [hep-ex].

[37] E. Komatsu *et al.* [WMAP Collaboration], Astrophys. J. Suppl. **180**, 330 (2009), arXiv:0803.0547 [astro-ph].

[38] G. Belanger, F. Boudjema, A. Pukhov and A. Semenov, Comput. Phys. Commun. **176**, 367 (2007) [arXiv:hep-ph/0607059].

[39] G. Jungman, M. Kamionkowski and K. Greist, Phys. Rep. **267**, 195 (1995); G. Bertone, D. Hooper and J. Silk, Phys. Rept. **405**, 279 (2005).

[40] J. R. Ellis, A. Ferstl and K. A. Olive, Phys. Lett. B **481**, 304 (2000).

[41] D. Hooper, arXiv:0901.4090 [hep-ph].

[42] P. Gondolo, J. Edsjo, P. Ullio, L. Bergstrom, M. Schelke and E. A. Baltz, JCAP **0407**, 008 (2004).

[43] H. Ohki *et al.*, Phys. Rev. D **78**, 054502 (2008) [arXiv:0806.4744 [hep-lat]].

[44] J. R. Ellis, K. A. Olive and C. Savage, Phys. Rev. D **77**, 065026 (2008) [arXiv:0801.3656 [hep-ph]].

[45] T. Sjostrand, S. Mrenna and P. Z. Skands, JHEP **0605**, 026 (2006) [arXiv:hep-ph/0603175].

[46] F. Stoehr, S. D. M. White, V. Springel, G. Tormen and N. Yoshida, Mon. Not. Roy. Astron. Soc. **345**, 1313 (2003) [arXiv:astro-ph/0307026].

[47] I. Cholis, G. Dobler, D. P. Finkbeiner, L. Goodenough, T. R. Slatyer and N. Weiner, arXiv:0907.3953 [astro-ph.HE].

[48] J. F. Navarro, C. S. Frenk and S. D. M. White, Astrophys. J. **462**, 563 (1996) [arXiv:astro-ph/9508025].

[49] J. Diemand, M. Kuhlen, P. Madau, M. Zemp, B. Moore, D. Potter and J. Stadel, Nature **454**, 735 (2008) [arXiv:0805.1244 [astro-ph]].

[50] J. F. Navarro *et al.*, arXiv:0810.1522 [astro-ph].

[51] F. Prada, A. Klypin, J. Flix Molina, M. Martinez and E. Simonneau, Phys. Rev. Lett. **93**, 241301 (2004) [arXiv:astro-ph/0401512]; Y. Mambrini, C. Munoz, E. Nezri and F. Prada, JCAP **0601** (2006) 010 [arXiv:hep-ph/0506204].

[52] A. A. Abdo *et al.* [The Fermi-LAT collaboration], Phys. Rev. Lett. **104**, 101101 (2010) [arXiv:1002.3603 [astro-ph.HE]].

[53] E. A. Baltz and J. Edsjo, Phys. Rev. D **59**, 023511 (1998) [arXiv:astro-ph/9808243].

[54] A. W. Strong and I. V. Moskalenko, arXiv:astro-ph/9812260.

[55] J. Lavalle, J. Pochon, P. Salati and R. Taillet, Astron. Astrophys. **462**, 827 (2007) [arXiv:astro-ph/0603796].

[56] D. Maurin, R. Taillet, F. Donato, P. Salati, A. Barrau and G. Boudoul, arXiv:astro-ph/0212111.

[57] D. Maurin, R. Taillet and C. Combet, arXiv:astro-ph/0609522.

[58] D. Maurin, R. Taillet and C. Combet, arXiv:astro-ph/0612714.

[59] J. Lavalle, Q. Yuan, D. Maurin and X. J. Bi, Astron. Astrophys. **479**, 427 (2008) [arXiv:0709.3634 [astro-ph]].

[60] Y. Mambrini, C. Munoz and E. Nezri, JCAP **0612**, 003 (2006) [arXiv:hep-ph/0607266].

[61] E. A. Baltz, J. Edsjo, K. Freese and P. Gondolo, Phys. Rev. D **65**, 063511 (2002) [arXiv:astro-ph/0109318].

[62] W. de Boer, C. Sander, M. Horn and D. Kazakov, Nucl. Phys. Proc. Suppl. **113**, 221 (2002) [arXiv:astro-ph/0207557].

[63] D. Hooper, A. Stebbins and K. M. Zurek, Phys. Rev. D **79**, 103513 (2009) [arXiv:0812.3202 [hep-ph]].

[64] F. Donato, D. Maurin, P. Salati, A. Barrau, G. Boudoul and R. Taillet, Astrophys. J. **563**, 172 (2001) [arXiv:astro-ph/0103150].

[65] C. Goy [AMS Collaboration], J. Phys. Conf. Ser. **39**, 185 (2006).

[66] *et al.* [PAMELA Collaboration], arXiv:1007.0821 [astro-ph.HE].

[67] I. Cholis, arXiv:1007.1160 [astro-ph.HE].

[68] O. Adriani *et al.*, Phys. Rev. Lett. **102**, 051101 (2009) [arXiv:0810.4994 [astro-ph]].

[69] I. V. Moskalenko, A. W. Strong, J. F. Ormes and M. S. Potgieter, Astrophys. J. **565**, 280 (2002) [arXiv:astro-ph/0106567].

[70] M. Cirelli and A. Strumia, New J. Phys. **11**, 105005 (2009) [arXiv:0903.3381 [hep-ph]].

[71] [Tevatron Electroweak Working Group and CDF Collaboration and D0 Collab], arXiv:0903.2503 [hep-ex].

[72] U. Chattopadhyay, D. Das, D. K. Ghosh and M. Maity, arXiv:1006.3045 [hep-ph].

[73] C. Amsler *et al.* [Particle Data Group], Phys. Lett. B **667**, 1 (2008).

[74] E. A. Baltz *et al.*, JCAP **0807**, 013 (2008) [arXiv:0806.2911 [astro-ph]].

[75] N. Bernal and A. Goudelis, JCAP **1003**, 007 (2010) [arXiv:0912.3905 [hep-ph]].

[76] J. Kopp, T. Schwetz and J. Zupan, JCAP **1002**, 014 (2010) [arXiv:0912.4264 [hep-ph]].

[77] N. Bernal, A. Goudelis, Y. Mambrini and C. Munoz, JCAP **0901** (2009) 046 [arXiv:0804.1976 [hep-ph]]; A. M. Green, JCAP **0807** (2008) 005 [arXiv:0805.1704 [hep-ph]]; L. E. Strigari and R. Trotta, JCAP **0911** (2009) 019 [arXiv:0906.5361 [astro-ph.HE]]; J. Billard, F. Mayet and D. Santos, arXiv:1006.3513 [astro-ph.CO].

[78] J. Engel, Phys. Lett. B **264**, 114 (1991).

[79] G. Duda, A. Kemper and P. Gondolo, JCAP **0704**, 012 (2007) [arXiv:hep-ph/0608035].

[80] M. Weber and W. de Boer, arXiv:0910.4272 [astro-ph.CO].

[81] P. Salucci, F. Nesti, G. Gentile and C. F. Martins, arXiv:1003.3101 [astro-ph.GA].

[82] M. Vogelsberger *et al.*, arXiv:0812.0362 [astro-ph].

[83] C. McCabe, arXiv:1005.0579 [hep-ph].

[84] A. M. Green, arXiv:1004.2383 [astro-ph.CO].

[85] D. Tucker-Smith and N. Weiner, Phys. Rev. D **64**, 043502 (2001) [arXiv:hep-ph/0101138]; D. Tucker-Smith and N. Weiner, Nucl. Phys. Proc. Suppl. **124**, 197 (2003) [arXiv:astro-ph/0208403].